

# The existence of a lateral size effect and the relationship between indentation and scratch hardness in copper

Kareer, A., Hou, X., Jennett, N. M., Hainsworth, S. V.

Author post-print (accepted) deposited by Coventry University's Repository

**Original citation & hyperlink:**

Kareer, A, Hou, X, Jennett, NM & Hainsworth, SV 2016, 'The existence of a lateral size effect and the relationship between indentation and scratch hardness in copper'

Philosophical Magazine, vol 96, no. 32-34, pp. 3396-3413. DOI:

10.1080/14786435.2016.1146828

<https://dx.doi.org/10.1080/14786435.2016.1146828>

DOI 10.1080/14786435.2016.1146828

ISSN 1478-6435

ESSN 1478-6443

Publisher: Taylor & Francis

*This is an Accepted Manuscript of an article published by Taylor & Francis in Philosophical Magazine on 2016 available*

*online: [http://www.tandfonline.com/Article 10.1080/14786435.2016.1146828](http://www.tandfonline.com/Article/10.1080/14786435.2016.1146828)*

Copyright © and Moral Rights are retained by the author(s) and/ or other copyright owners. A copy can be downloaded for personal non-commercial research or study, without prior permission or charge. This item cannot be reproduced or quoted extensively from without first obtaining permission in writing from the copyright holder(s). The content must not be changed in any way or sold commercially in any format or medium without the formal permission of the copyright holders.

This document is the author's post-print version, incorporating any revisions agreed during the peer-review process. Some differences between the published version and this version may remain and you are advised to consult the published version if you wish to cite from it.

# **The existence of a lateral size effect and the relationship between indentation and scratch hardness in copper**

A. KAREER, X. D. HOU, N. M. JENNETT and S. V. HAINSWORTH

1. Department of Engineering, University of Leicester, University Road, Leicester, LE1 7RH, UK
2. Materials Division, National Physical Laboratory, Teddington Middlesex TW11 0LW, UK
3. Faculty of Engineering, Environment and Computing, Coventry University, Coventry, UK

## **Abstract**

Indentation size effects are well known in static indentation of materials that deform by dislocation based mechanisms. However, whilst instrumented indentation techniques have become rapidly established as a means of determining the near-surface mechanical properties of materials, scratch testing has been much less widely used. Hardness is used in wear models as a proxy for the yield stress, and the design of materials and hard coatings has often sought to exploit size-derived performance enhancements through length-scale engineering. Yet, it is not known directly whether (or not) length-scale effects also apply to scratch (and thus wear) performance at small scales, or what the functional form of this effect is. This work directly demonstrates that there is a lateral size effect and shows that there are questions to be answered if the use of hardness as an indicator of wear performance is to remain valid.

We report on constant load scratch experiments using a Berkovich indenter on single-crystal, annealed copper, using a range of applied normal forces, and compare results from three scratch hardness calculation methods to indentation hardness (ISO 14577:2002) measured on the same sample at the same loads. Scratch tests were performed with the Berkovich indenter aligned either edge-forward or face-forward to the scratch direction. In all cases we demonstrate that there is a very significant (approximate factor of two) effect of scratch size (a lateral size effect) on scratch hardness. The results also show that the deformation mechanisms occurring in scratch tests are different to those occurring beneath a static indentation and that different mechanisms dominated for different stylus orientations (face-forward vs. edge-forward orientation). This is, to our knowledge, the first direct demonstration of a lateral size effect akin to the indentation size effect in metallic materials. The results have significant implications for using static indentation as a predictor of deformation during wear processes.

Keywords: nano-scratch testing, nano-scratch hardness, lateral size effects

## **1. Introduction**

Hardness testing has evolved from early empirical attempts to rank which materials are ‘stronger’ and can damage other ‘weaker’ materials. One early hardness scale is the Moh’s hardness scale, where it is the ability of one material to *scratch* another that is ranked. Simplification of the scratch test to a single point force application has brought us the widely useful, and more reproducible indentation hardness test. This expresses hardness as a plastic yield pressure that is analogous to the uniaxial yield stress and proof/flow stress found in mechanical compression testing. Tabor 1951 [1] showed that plotting Brinell indentation

pressures as a function of the geometrically applied indentation strain yields a curve that can be overlaid onto a compression stress-strain curve. Hardness testing standards require the use of “self-similar” geometries so that a constant indentation strain is generated at any indentation depth; the base assumption being that the hardness value obtained is unique at any particular strain and, therefore, should be constant with indentation penetration. Hardness is a simpler test than scratch, being static rather than dynamic, and acting in only one direction. It is, therefore, not surprising that hardness testing is often used to specify a material and/or to indicate the likely friction and wear of a surface or coating, epitomised by the well-known Archard’s Law [2]. Although scratch testing of coatings has been widely used [3]–[8], the scratch test standards that have been developed are mainly devoted to the characterisation of coating fracture and adhesion and there is a relative neglect of scratch as a means to determine hardness [9]. Indeed, a length-scale independent, “continuum mechanics” approach to the strength of materials suggests that the yield of a material is direction independent (except for crystallographic anisotropy) and that scratch and indentation can be considered as essentially equivalent. Wredenberg and co-workers have previously compared indentation hardness and scratch hardness of both metallic and polymeric materials and found that the scratch response was closely related to the Johnson model, which is used to categorise the indentation response of a material into three distinct stages [10]. Bellemare and co-authors have related elasto-plastic parameters (Young’s modulus, yield stress, power law hardening exponent), to the steady state frictional sliding response using both computational and experimental methods [11].

It is, however, now known that yield stress and hardness are not invariant responses to a particular strain but, in fact, scale with a critical dimension that is the average spatial frequency of all obstacles (in a material and-or test geometry) that act to constrain the size of a dislocation source or to hinder the movement of dislocations [12]. In particular, the size of the plastic volume generated in a hardness test is itself related to the hardness value measured; “smaller is harder” and a Hall-Petch-like Indentation Size Effect (ISE) is observed [13], [14]. The plastic deformation in a scratch is not the same as that under an indentation and, therefore, this work investigates the relationship between indentation hardness and scratch hardness, and whether there is, in fact, a scratch or lateral size effect akin to ISE. Beake and co-workers have identified the importance of understanding the size effects observed in scratch testing from work carried out on biomaterials used for hip joints, in which small scale scratches (approx.  $<1\mu\text{m}$  deep) were observed to produce significant wear and eventually failure of the joints [15].

In this paper we analyse the response of pure, single crystal copper to scratches performed by an instrumented (nano-)indentation tester (IIT) using a Berkovich diamond indenter. We compare different methods by which a scratch hardness value can be determined and demonstrate that lateral size effects exist in scratch hardness testing. The scratch hardness results and size effects are also compared to the size-dependent indentation hardness results obtained on the same sample.

#### *Scratch Hardness Number, $H_s$*

Three methods to determine the scratch hardness of a scratch performed by an instrumented indentation tester are used and compared; all being variations of the basic pressure calculation

of *Force/Area*. The methods are explained below and are shown diagrammatically in Figure 1. The stylus used was a Berkovich Indenter, whose geometry is an equilateral triangular-based pyramid. This geometry simplified the assumptions of the angle and area of contact of the indenter with the scratch track. The indenter was aligned to the scratch direction so that either, exactly one facet (face forward, or FF), or exactly two facets (edge forward, or EF) were in contact during the scratch formation. Care was taken that the tip was well aligned, as a variation in the angle of attack would result in a more complex deformation mechanism.

*Method one,  $H_s(1)$* : The standard ASTM G171 test defines the scratch hardness number as the normal force of a constant-force scratch, divided by the projected area of contact, which is taken as a semi-circle with the diameter being the width of the scratch track (as measured directly from the residual scratch impression [16]). The scope of the ASTM test is restricted to macroscopic scratch tests performed with a Rockwell sphero-conical diamond indenter. Method one takes a similar analytical approach and defines the Berkovich scratch hardness,  $H_s(1)$  as a constant normal force,  $F_N$ , divided by the projected area of contact of the indenter with the scratch track. For IIT-based scratch instruments, the scratch penetration depth is measured from the indenter displacement channel. This may be used as the contact depth from which to calculate the projected contact area of the whole tip at that depth,  $A_p$ . Depending on the orientation of the tip during the scratch, however, different proportions of the tip are in contact with the material during the scratching process. If the projected area of the indenter at any particular indentation depth is  $A_p$ , then, in a FF scratch, the projected area of scratch contact is one third of  $A_p$ . Similarly, in an EF scratch, the contact area is two-thirds of  $A_p$ .

*Method two,  $H_s(2)$* : This method was designed to be representative of the lateral resistance of the material.  $H_s(2)$  is defined as the measured lateral force,  $F_L$ , divided by the lateral area of contact,  $A_T$ . This lateral contact area is the area of the cross-section of a scratch and is the same at any given scratch depth for both EF and FF tip orientations (directions of motion). For comparison with method one, the facet side length of the indenter at the scratch penetration depth distance from the tip is used and an isosceles triangle assumed.

*Method three,  $H_s(3)$* : This method takes a “free body” approach of force balance on the stylus, such that the material resistance balances the combination of a normal and a lateral force on the scratching stylus. The normal force and the lateral force are, therefore, resolved to give a reaction force,  $F_r$ , acting on the facet(s) of the indenter. When scratching in the FF orientation,  $F_r$  acts on the surface area of a single facet in contact with the scratch (see Figure 1.d). For the EF orientation, the reaction force is assumed equally split between the two facets in contact, at an in-plane separation angle of  $60^\circ$  (see appendix 1). Further details of how the values of area were determined from the nano-scratch data are given in the experimental details section.

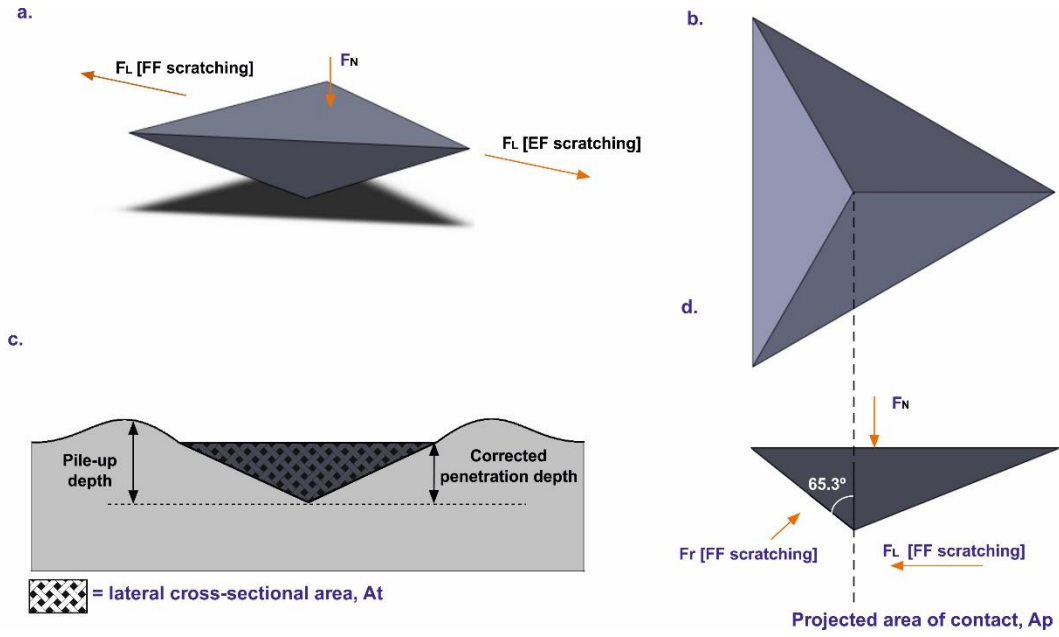


Figure 1: Diagrams to show: a) The tip orientation for edge forward (EF) and face forward (FF) scratches. Lateral force,  $F_L$  acts in the direction of motion. b) The projected area of contact used in the calculation of  $H_s(1)$ , one third  $A_p$  is used for FF and two thirds  $A_p$  is used for the EF c) Cross-section of the scratch; the corrected penetration depth is shown by the hatched area. The pile-up depth, which is the unloaded actual lateral cross-sectional area as measured directly using atomic force microscopy (AFM) is also shown. The lateral area,  $A_t$ , used in  $H_s(2)$  is the dark area. d) The resolved force,  $F_r$ , for a FF scratch as used in the calculation of  $H_s(3)$ .

## 2. Experimental Details

### *Sample Preparation*

A sample of single-crystal, oxygen-free, pure copper (99.9% purity) oriented in the (100) crystallographic plane (obtained from Goodfellow UK) was used for these experiments. The sample was annealed in air for 4 hours at 600°C, then mechanical- and electro-polished in order to obtain a smooth flat surface, with negligible residual stresses.

### *Instrumented (Nano)-indentation tests*

Instrumented (nano)-indentation experiments were performed using an Agilent G200™ instrumented indentation tester fitted with a Berkovich diamond indenter tip. The BS EN ISO 14577:2002 method was adopted to determine the indentation hardness [17]. Indentation, peak loads used were in the range of 0.5 mN - 40 mN; 10 repeats at each force were performed and the data averaged. The time to peak load was 15 seconds for all normal loads and therefore the loading rate and unloading rates were specific to the maximum peak load for that test then held at peak load for 10 seconds before unloading, and a 60 second hold at 90% unloading for the assessment of thermal drift.

### *Instrumented (Nano)-scratch tests*

Scratch tests were performed using the same Agilent G200™ instrumented indentation system fitted with a lateral force measurement probe and the same Berkovich diamond indenter tip. The indenter tip-shape was measured, directly, using a metrological atomic force microscope (AFM) (Park Autoprobe M5, Veeco instruments, Pasadena, CA), before any scratches were made. Two expressions for the indenter area function were derived from the AFM data: one gave the projected area of contact as a function of depth; the second gave the surface area of contact as a function of depth.

A ‘three-pass’ scratch method was used with a constant normal scratch force:

- The first pass profiled the surface topography at a low force. A 20% over-scan at the beginning and end of the scratch segment provided a reference surface position;
- The second pass was the scratch segment and was performed at the profiling force until the start of the scratch was reached. Here the force was increased to the scratch force, whilst the stylus was stationary, then the scratch performed at the scratch force for the length of the scratch (100  $\mu\text{m}$  in the centre of the profiled region). The force was then returned to the profiling force for the remainder of the over-scan region.
- The third pass profiled the surface again, at the low profiling force, to give the residual topography of the surface, including the 20% over-scanned regions.

The difference between the first pass profile and second pass scratch segment provided the ‘corrected penetration depth’ i.e. the scratch penetration depth beneath the original topography of the surface. Scratch normal forces used for this experiment ranged from 0.5 mN to 40 mN and the profiling force used was 0.1 mN. The velocity of the tip during each scratch was 10  $\mu\text{m/s}$  and all scratches were 100  $\mu\text{m}$  in length, plus two overscan regions, of 20  $\mu\text{m}$  each, at the beginning and end of the scratch. Five repeats of each scratch were performed and the data averaged.

### 3. Data analysis and scratch hardness calculations

Figure 2 shows a typical scratch profile of a scratch made using a normal force of 20 mN. For each scratch the transition between profiling force and scratch force occurs at a single point, at the start of the scratch, (Position 1). Effectively, an indentation is made at this position to reach the required force. The footprint of the indentation extends outwards, as the indentation evolves, and can be seen to overlap the remnant pre-scan scratch in the case of the EF scratch shown in Figure 3 (top). The scratch penetration depth at Position (1) agreed well with the indentation depth obtained in pure indentation tests at the same normal force, on the same sample (see Figure 6.a). Once the full scratch force is reached, the indenter then moves laterally with respect to the sample to create the scratch and the lateral force is measured using lateral force measurement (LFM) probes (see appendix 2). Two opposing things therefore happen at the start of the scratch:

- The indenter is pulled sideways so that the back facet(s) of the indenter move(s) away from the initial indentation contact. The amount of surface supporting the indentation force is therefore reduced; as a result, the vertical force can no longer be supported

and the indenter starts to penetrate deeper to maintain the contact area necessary to support the applied force.

- Resistance to the lateral movement builds up as the material ahead of the indenter is forced to flow around it. This resistance pushes against the leading facet(s) of the indenter, which generates an upward component of force. Figure 2 suggests that this also acts to reduce the scratch depth (and so contact area) needed to support the normal force. Since the area required to support the same force is reduced, the apparent hardness of the material must increase. The extent of this effect is likely to depend on the scratch speed and the facet angle; as a result, the scratch depth can be more or less than the static indentation depth.

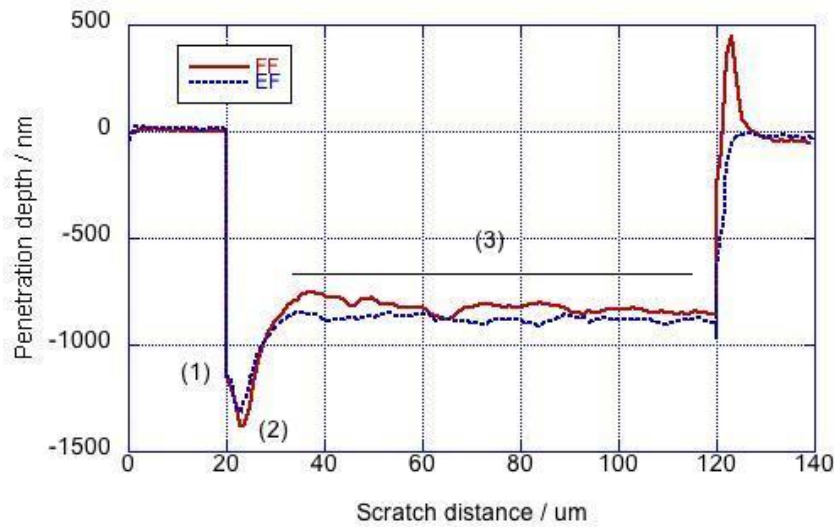


Figure 2: Typical scratch penetration depth channel data comparing the two different scratch types: edge forward (EF) and face forward (FF). Normal applied force is  $F_{\max} = 20$  mN. Position (1) is the indentation depth when the normal force of 20 mN is reached. Position (2) is defined as the maximum penetration depth at the beginning of the scratch after the indenter starts to move laterally. Region (3) is the steady state scratch response at constant applied force and scratch speed.

The combination of the above two effects resulted in a net scratch penetration depth increase followed by a reduction, for both the EF and FF scratches, as clearly demonstrated in Figure 2; position 2 is defined as the maximum penetration depth achieved due to the combination of these two effects, at the beginning of the scratch. The FF direction, in particular, suffered a more rapid loss of indentation support than an increase in lift due to lateral motion. However, once the laterally induced lift is fully developed, the indenter “climbs out of” the initial indentation, and enters into a “steady-state region”, illustrated as “region (3)”. Since the initial transition is affected by stylus orientation, scratch direction and scratch speed etc., an improved estimate of the average scratch depth was obtained by excluding this region from analysis and averaging the parameter values measured in the “*steady-state* region” of the scratch; this gave more reliable average values for scratch penetration depth,  $h$ , normal force,  $F_N$ , and lateral force,  $F_L$ .

Calculation of  $H_s(1)$ : The average steady state corrected penetration depth (Figure 2 region(3)),  $h$ , was substituted into the indenter tip projected area function and the resulting

total projected area (see Figure 1.b) scaled according to the number of contacting facets, depending on the orientation of the tip during the scratch.

Calculation of  $H_s(2)$ : The lateral cross-sectional area,  $A_T$ , shown in Figure 1.c. was calculated using the projected area of contact at the average steady state penetration depth (Figure 2, region (3)) to determine the length of one side of the projected equilateral triangle. This was used as the scratch width, and the corrected penetration depth was used as the height of the lateral cross-section triangle,  $A_T$ . An estimation of the tip rounding was generated to correct for the tip not being perfectly sharp and thus  $A_T$  not being a perfect triangular cross-section.

Calculation of  $H_s(3)$ : The averaged  $F_N$  and  $F_L$  were resolved to give an average  $F_r$ , acting on one facet in the FF orientation and two facets in the EF orientation (see Figure 1.d for FF and see appendix 1 for EF  $F_r$  calculations). The average steady state penetration depth (Figure 2, region (3)),  $h$ , was substituted into the indenter tip surface area function and the resulting total surface area scaled according to the number of contacting facets, depending on the orientation of the tip during the scratch.

Note that the corrected penetration depth used in the above calculations,  $h$  is the penetration of the indenter beyond the original surface position and, therefore, does not include any pile-up generated.

## 4. Results

Figure 3 contains 3D representations of AFM scans of an edge forward (EF) 20mN scratch and a 20mN face forward (FF) scratch with arrows to show the stylus direction of scratching. A small scratch that is overwritten by the main scratch can be seen. This is due to the pre-scan force exceeding the elastic limit of the surface and a permanent plastic impression being left as a consequence.

Figure 4 shows AFM 2D and 3D representations and a line profile of a small portion of the central section of the same scratches as in Figure 3.



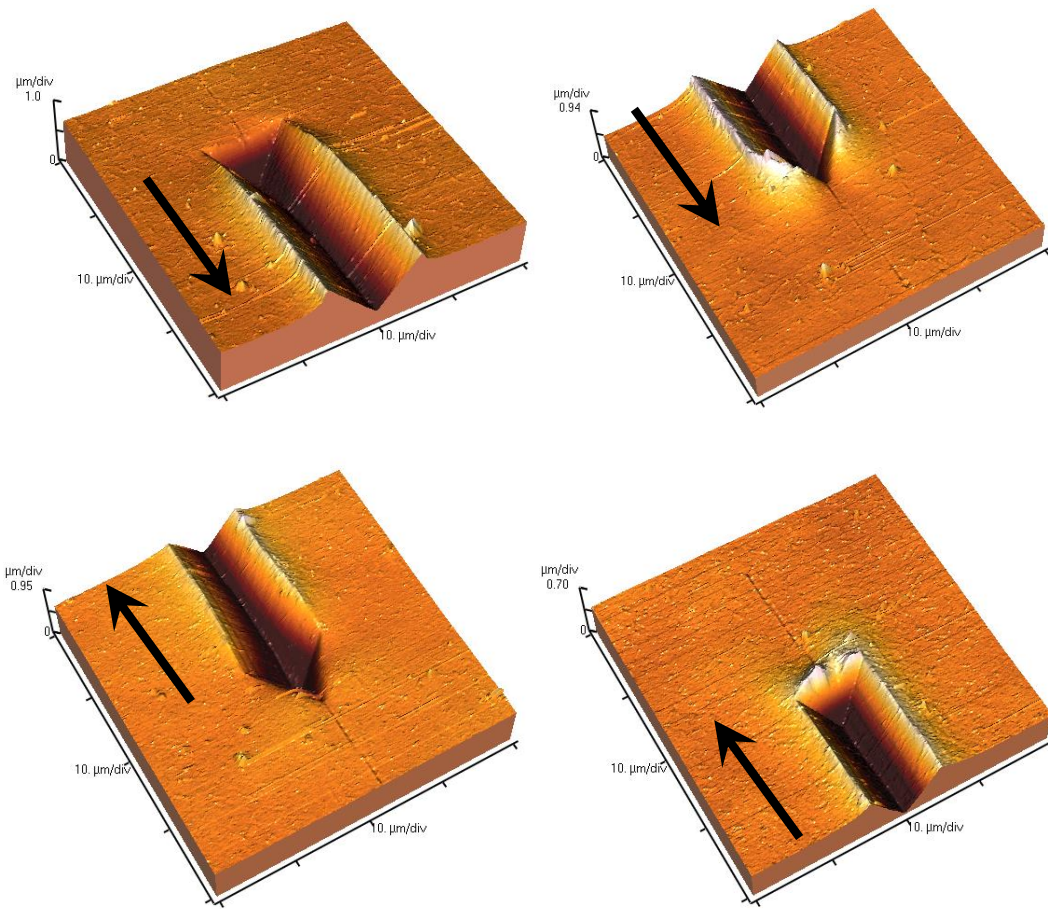
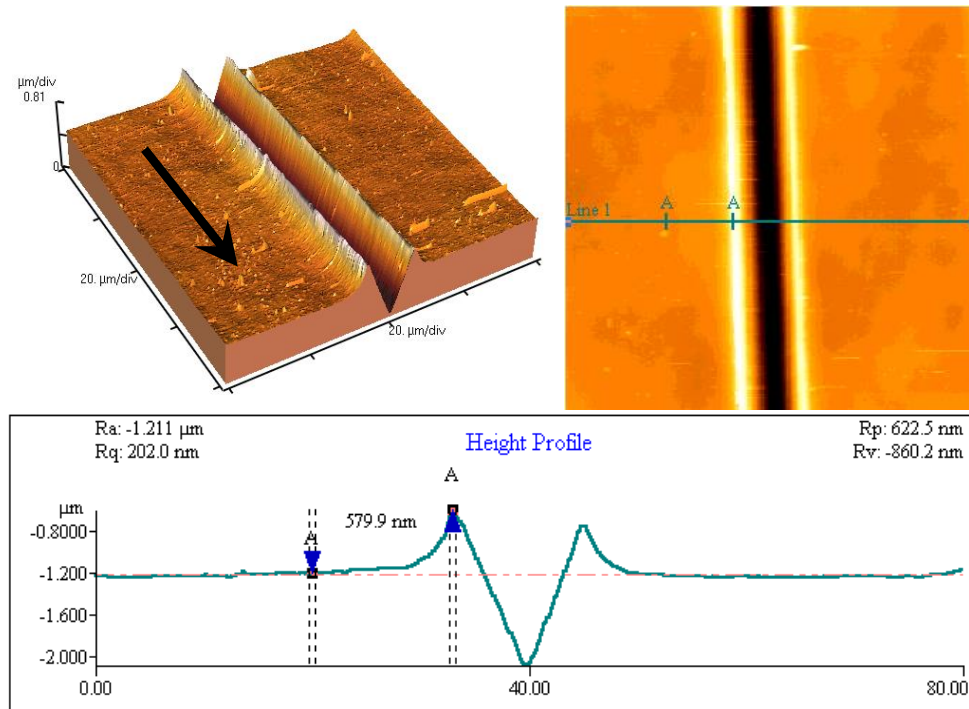


Figure 3 Top: AFM images of the start and end of an edge forward scratch with a 20mN normal force.  
 Bottom: AFM images of the start and end of a face forward scratch with a 20mN normal force.  
 The arrow marks the (stylus) direction of scratching. Note the difference in topography of the “terminal moraine” at the end of the scratch for the different directions of scratching. The smaller scratch is due to the pre-scan force exceeding the elastic limit of the surface and leaving a permanent plastic impression.

a)



b)

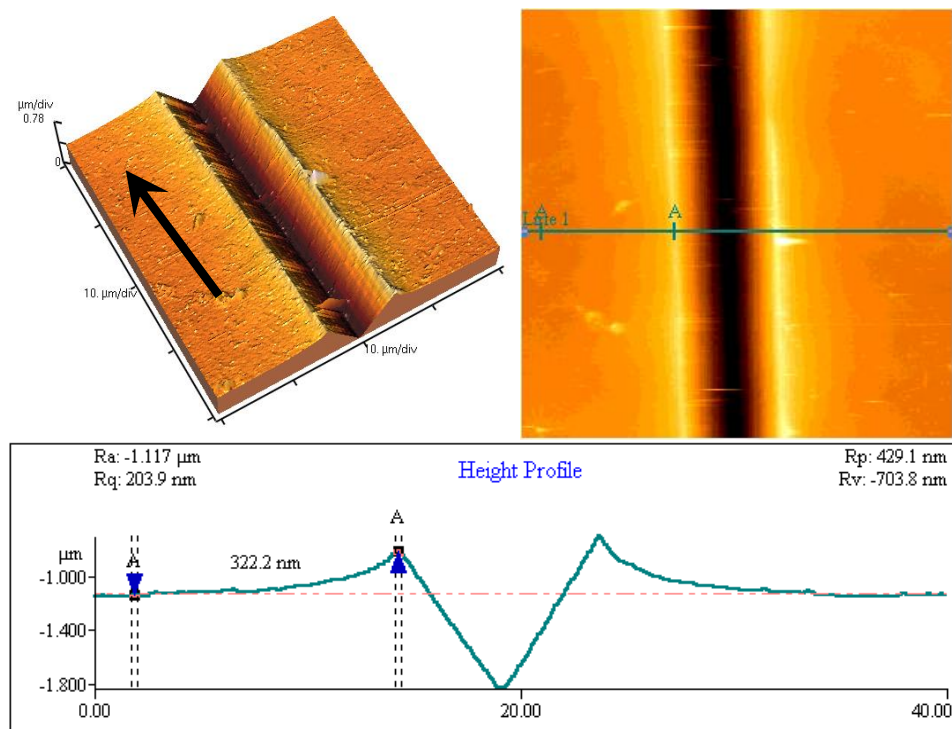


Figure 4: a) AFM scan of the middle of the Edge Forward scratch in Figure 2 with a linescan showing the amount of pile-up. b) AFM scan of the middle of the Face Forward scratch in Figure 2 with a linescan showing the amount of pile-up. Arrow indicates indenter scratching direction.

Averaged single values of the  $F_N$  and  $F_L$  for each scratch were obtained by averaging the data in the normal and lateral force channels for all positions within the steady state region of the scratch (region (3) in Figure 2); these values are plotted in Figure 5. In Figure 6, the penetration depth of the scratches at the three positions defined in Figure 2 are plotted; the depth of indentations performed at equivalent normal forces are additionally plotted in Figure 6.a and compared to the depth of the scratch upon initial loading, when all three facets of the indenter are in contact and there is no lateral motion i.e. a static indentation is being performed. Figure 6.b shows the ratio of the depth at position(2)/(1) as defined in Figure 2; this is the relative increase in penetration depth to compensate for the reduction in contact area as the indenter loses either one or two facets of contact. Figure 6.c shows the averaged penetration depth in the steady state region for both the face forward and edge forward scratches.

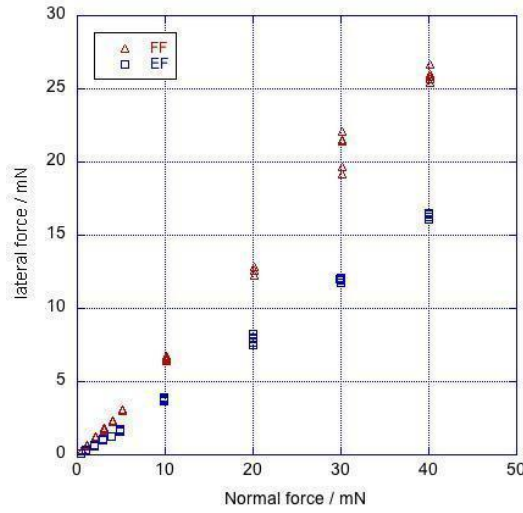
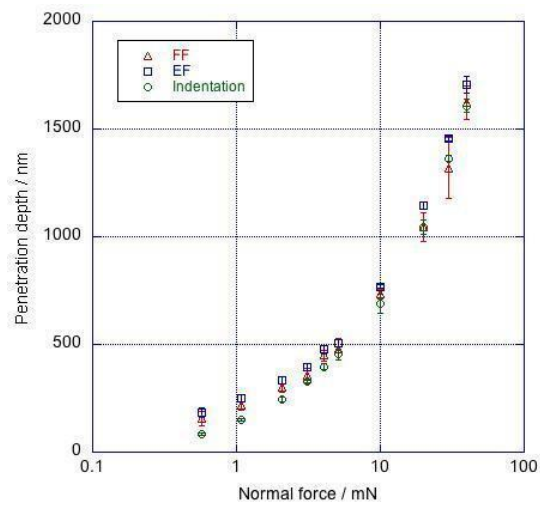
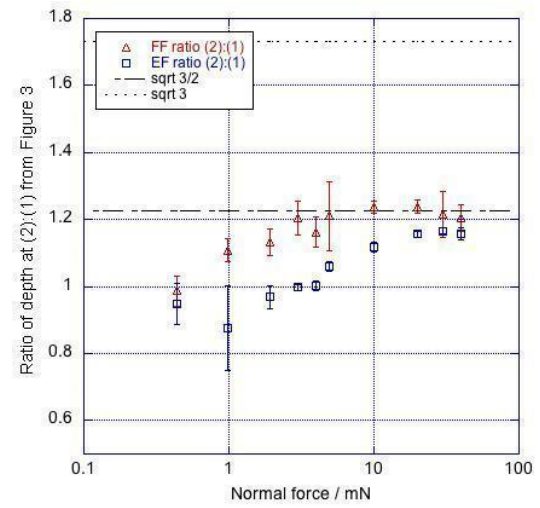


Figure 5: Normal force vs. Lateral force. All data are averaged throughout the steady-state region for each scratch performed. Each data point is an average of 5 repeat scratches and error bars represent one standard deviation. The dependence of the ratio of lateral to normal force on scratch direction can be clearly seen.

a.



b.



c.

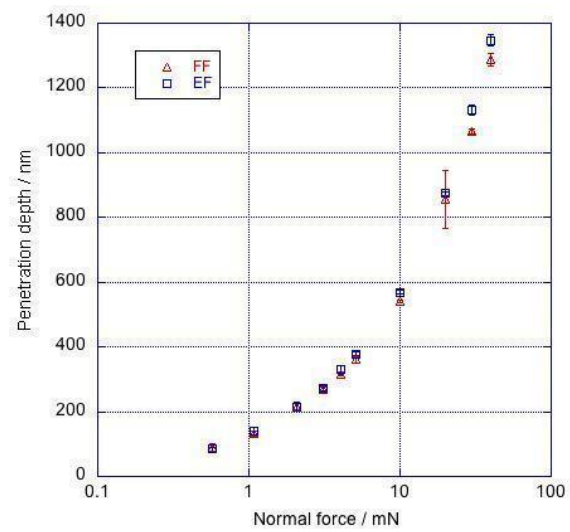


Figure 6: a) Plot of normal force vs. penetration depth at  $F_{max}$  for indentation and for scratch at position (1). b) ratio of depths position (2): position(1). c) Penetration depth averaged over region (3). Note that in all cases, data points represent the average of 5 scratches; error bars represent one standard deviation.

Values of the scratch hardness calculated using the three methods are shown in Figure 7, Figure 8 and Figure 9, together with the nano-indentation hardness of the same sample for comparison. All scratch hardness values were calculated for the five repeat scratches in each case and averaged. The error bars represent a single standard deviation and it can be seen that the lower penetration depths have a greater degree of scatter, possibly due to sample roughness.

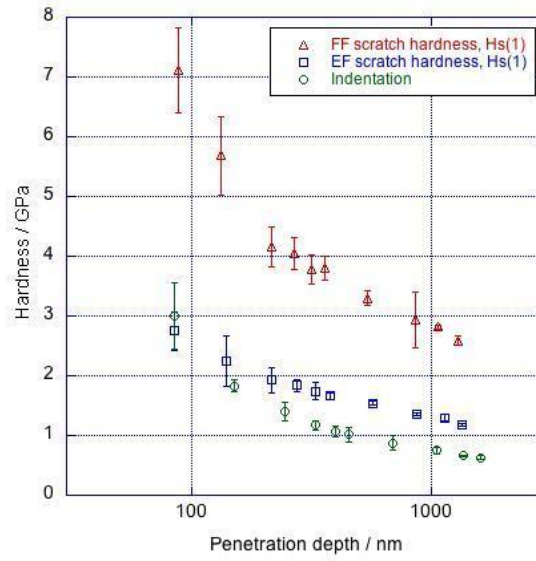


Figure 7: Scratch hardness measured using method  $Hs(1)$  vs. averaged penetration depth from region (3) in figure 2. Data points are average of five repeat scratches; error bars represent one standard deviation. Scratches were performed in both the face forward and edge forward tip orientations.

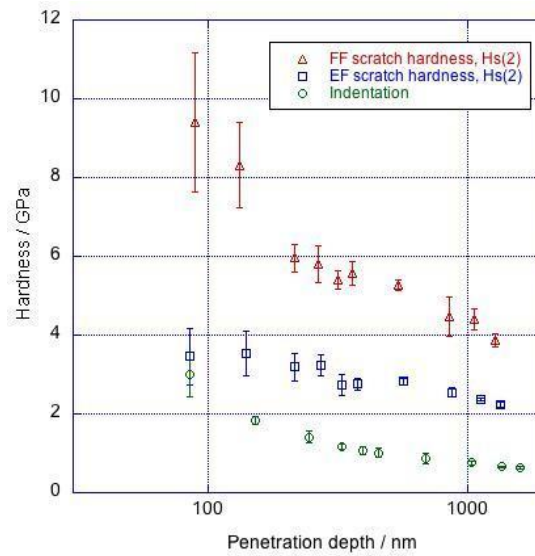


Figure 8: Scratch hardness measured using method  $H_s(2)$  vs. averaged penetration depth from region (3) in Figure 2. Data points are average of five repeat scratches; error bars represent one standard deviation. Scratches were performed in both the face forward and edge forward tip orientations.

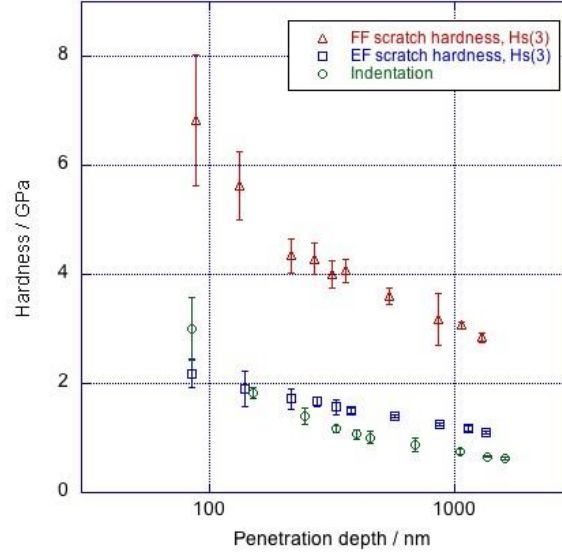


Figure 9: Scratch hardness measured using method  $H_s(3)$  for scratches performed in both the face forward and edge forward tip orientation. Hardness values presented are averages from the five repeat scratches; error bars represent one standard deviation.

## 5. Discussion

### 5.1. Scratch penetration depth

Figure 6.a shows that the penetration depth of the static indentation in the scratch, is unaffected by tip orientation and is approximately equal to the maximum penetration depth reached in indentation tests at the equivalent normal force. This is expected as in all three cases (FF scratch, EF scratch and indentation), the three facets of the indenter are providing support for the normal force, without generating any additional lateral forces. As the tip begins to traverse laterally across the sample, it is no longer in contact with the back wall of the scratch track. The normal force is therefore transferred from three facets of support, to either one (FF scratch) or two (EF scratch) facets, causing the indenter to penetrate further into the material. Figure 6.b shows, for all scratches, the ratio of the depth of the ‘initial maximum depth’ (position(2) of Figure 2) to the depth at which the normal force is supported by three facets at the maximum force (position(1) of Figure 2). In the FF case, the force is transferred to  $\frac{1}{3}$  of the contact area and therefore the depth might be expected to increase by a factor of  $\sqrt{3}$ . In the EF case, the contact area supporting the normal force is reduced to  $\frac{2}{3}$  of the contact area and therefore the depth might be expected to increase by a factor of  $\sqrt{\frac{3}{2}}$ . In a *steady state*, therefore, it might be expected that the FF scratch would be deeper than the EF scratch. Figure 6.b does show that there is an increase in depth from position(1) to



position(2), but that the increase in depth is less than expected, especially for the FF scratches.

In the dynamic *steady state*, (region(3) of Figure 2), there is little difference between the averaged depth of the EF and the FF scratches (see Figure 6.c). This is contrary to the expectations described above based on the number of facets supporting the normal force. The indenter can only rise up with lateral force if the material is genuinely harder, or some of the applied normal force is supported by a mechanism other than plastic yield stress of the materials. One explanation could be that the FF facet traps a volume of material under it, and high hydrostatic compressive forces are generated under the facet, which are supported by a wider area of surrounding material. A similar idea is that, in the face forward orientation, a volume of trapped material is ‘pushing’ through the sample and creating the scratch groove, rather than the single facet of the indenter. This would result in a larger surface area for the resolved scratch force to be acting on, which might make the lateral hardness appear higher than expected. The FF scratches can certainly be seen to leave a remnant pile-up of material at the end of the scratch track. Alternatively, the FF scratch could be causing greater work-hardening e.g. by causing displaced material to flow around a 90 degree corner, thereby undergoing more strain. Early 3D Finite element analysis of Berkovich-equivalent conical indenter scratches by Bucaille and Felder, certainly suggest that the representative strain around a scratch is greater than around the equivalent indentation [19]. In the EF case, the material flows outwards to the sides of the scratch groove along a shallower angle of 30 degrees. The larger lateral force exerted in the FF case means that a higher amount (and rate) of work is being done, which is consistent with the idea of more dislocation generation and therefore work-hardening occurring in FF scratches; higher (work induced) hardness would cause a lower penetration depth than expected. Similar differences, between the two tip orientations, are observed in the lateral force measurements (Figure 5) and the scratch hardness measurements (Figures 7-9).

## 5.2. Scratch Hardness

It can be seen from Figures 7-9 that the scratch response is a function of the orientation in which the tip is placed with respect to scratch direction, regardless of the method used to calculate scratch hardness. A lateral size effect (LSE) can also be seen in all cases, i.e. there is an increase in scratch hardness with decreasing penetration depth. This is similar to the indentation size effect which has been known for many years. The LSE trend is observed in all methods however the degree to which the hardness increases is different for FF and EF scratches and for the different scratch hardness calculation methods.

We compared three different definitions of scratch hardness. Method one was based on the macroscopic scratch hardness and we have shown that this produces scratch hardness values ranging from 2.6 GPa to 7.1 GPa (size effect ratio = 2.8) for scratches performed on the single crystal in the FF tip orientation and 1.2 GPa to 2.8 GPa (size effect ratio = 2.3) for the EF tip orientation. The second method measures the projected lateral pressure, which is acting perpendicularly to that measured in method one; however the general concept is analogous. For this method (two), scratch hardness values of 3.9 GPa to 9.4 GPa (size effect ratio = 2.4) for the FF tip orientation and 2.2 GPa to 3.5 GPa (size effect ratio 1.6) for the EF tip orientation were obtained. In all cases, the scratch hardness is significantly larger than the

indentation hardness measured in the normal direction. In method one, the lateral force component is being neglected and in method two the normal force has not been incorporated. Method three incorporates both forces into a resolved force acting normally on the facet(s), from which hardness values of 2.5 GPa to 6.1 GPa (size effect ratio = 2.4) were obtained for the FF tip orientation and 1.1 GPa to 2.2 GPa (size effect ratio = 2.0) were obtained for the EF tip orientation. In this case, the FF hardness was larger than the indentation hardness for all scratch sizes and the EF was larger than the indentation hardness for most scratches, excluding the smallest scratch sizes. If the lateral Size Effect (LSE) is generated by a change in local length-scale (as is thought to be the case in ISE [12]) then the higher LSE for FF scratches would seem to be further indication that the FF ‘ploughing’ is causing a larger increase in dislocation density (work hardening) and/or grain size reduction (twin boundary creation or dislocation cell net structures perhaps) than in the EF scratches.

The discrepancies between the indentation hardness and the scratch hardness results suggest that it is insufficient to use indentation hardness as the key metric for wear calculations. The resistance of the surface to a laterally traversed asperity is underestimated by using indentation hardness and use of the scratch test, and a scratch hardness parameter could be a more appropriate method to characterise the wear resistance of materials, whilst maintaining test simplicity.

It should be noted that all the scratch hardness analysis methods used here, determine the averaged corrected penetration depth during the steady-state scratch region and derive the contact area from knowledge of the indenter area function. This depth includes the plastic deformation of the contact, but not the pile-up. From direct measurements of the pile-up height, using AFM, it is evident that a large amount of material piles-up at the edges, and end of the scratch track; the amount of pile-up and the pile-up morphology depends on the tip orientation. When such direct measurements of the scratch depth (i.e. including the pile-up but not the elastic deformation) were used in the hardness calculations, it was found that the LSE trends remained the same and the hardness values only deviated slightly from the hardness values recorded here. Refinement of the method (to include the pile-up into the analysis) is difficult, as it becomes necessary to measure the residual scratches directly, but an analysis based on the Oliver and Pharr method [18] using the unloading curves at the end of the scratch segment could perhaps be performed to give the contact depth  $h_c$ . When  $h_c$  is substituted into the area function, it would give a better estimate of the area of contact. If the elastic modulus could be obtained from the initial indentation, by a suitable partial unload step, then back calculation of a pile-up corrected  $h_c$  could be done by substituting the modulus and the unloading stiffness into the usual indentation stiffness equation [18].

The purpose of this work was to investigate the length-scale dependence of scratch hardness. A Berkovich geometry stylus was selected because this allowed the assumption that the resolved force was uniformly distributed across the flat facets. The angle of the facet(s) is known, thus the magnitude and direction of the resolved force, in each tip orientation, could be identified; essentially making this method of calculating scratch hardness unique. This would not be possible with a spherical or conical probe, which has a much more complex distribution of strain ahead of the indenter, as is noted by those who have used this geometry in models [19]. The use of a large spherical tip for scratch experiments, could be useful, at low forces, if the aim was to keep the stresses beneath the indenter below the elastic limit,



thereby allowing the investigation of tribological properties in the absence of plasticity. However, as soon as plasticity occurs and, consequently, the indenter begins to lose contact with the material at its trailing edge, contact area definition becomes an issue.

## 6. Conclusions

- The results clearly demonstrate that a lateral size effect exists for scratches on single crystal copper. The scratch hardness increases with decreasing depth of penetration for both face-forward (FF) and edge-forward (EF) scratching orientations regardless of the definition used for scratch-hardness. The lateral size effect is consistently larger for FF scratches than for EF scratches.
- Three different methods were used to calculate the scratch hardness and, in all cases the face forward scratch hardness was approximately double that of the edge forward orientation scratch hardness. In turn, the edge forward scratch hardness was consistently harder than the indentation hardness at each applied normal force.
- Two of the scratch hardness calculation methods used a simple approach of dividing either the normal force by the normal contact area or the lateral force by the lateral cross-sectional area. Owing to the more complex deformation of the scratch experiment, neither method is a completely satisfactory description of the scratch response; it is more physically meaningful to use the resolved force on the facet to determine the nano-scratch hardness. This third method uses a resolution of both the applied normal load and lateral force divided by the facet surface area of contact. This is a simple calculation for a Berkovich indenter but not for an axially symmetric indenter. Thus, although the same issues would apply to measuring scratch hardness when using a spherical/conical indenter, resolving the two force components for these tip geometries would induce further calculation complexities.
- The penetration depth of the stylus is dependent on the lateral force generated as well as the area of contact with the scratch surface. This suggests that additional load support is being generated via the lateral force. It is unclear why this happens, but additional mechanical work is done indicating additional plastic work is being done e.g. in dislocation generation or material flow/pile-up. This is consistent with literature FEA analysis indicating that an indenter generates increased representative strain during a scratch test than during indentation [19].
- Further investigation is necessary to determine the exact underlying deformation mechanisms and flow of material ahead of the indenter as a function of scratch stylus orientation to scratch direction. In the interim it is recommended to perform the experiment with both tip orientations, as this provides additional information regarding the lateral resistance to plastic deformation.
- Using only indentation hardness to understand wear mechanisms clearly underestimates the resistance of a material to a single asperity contact traversing laterally across a surface.
- The practical implication of the scratch results presented here, is that it is currently not possible to assign an absolute scratch hardness. Not only does the geometry of the indenter have to be specified, but the orientation of the scratch direction must be defined before sets of scratch results can be compared.

- Use of any hardness value as an indicator of material strength, durability and wear resistance requires modification to take account of plasticity size effects. To do this, the relationship between ISE and LSE is required. Here it is shown that the functional form of the LSE is different to that of ISE if the same indicative length scale parameters, as used in indentation, are used for the comparison.

## Acknowledgments

This research was supported by funding for the National Physical Laboratory from the National Measurement Office of the UK Government Department for Business, Innovation and Skills.

## References

- [1] F. P. Bowden and D. Tabor, *The Friction and Lubrification of Solids*, Vol.1 ed. Clarendon Press, Oxford.
- [2] J. F. Archard, "Friction between metal surfaces," *Wear*, vol. 113, no. 1, pp. 3–16, 1986.
- [3] S. J. Bull, "Failure mode maps in the thin film scratch adhesion test," *Tribology International*, vol. 30, pp. 491–498, 1997.
- [4] P. A. Steinmann, Y. Tardy, and H. E. Hintermann, "Adhesion testing by the scratch test method: The influence of intrinsic and extrinsic parameters on the critical load," *Thin Solid Films*, vol. 154, no. 1–2, pp. 333–349, 1987.
- [5] J. Valli, "A review of adhesion test methods for thin hard coatings," *J. Vac. Sci. Technol. A Vacuum, Surfaces, Film.*, vol. 4, no. 1986, p. 3007, 1986.
- [6] S. J. Bull, "Tribological and micro-tribological phenomena in coatings," in *Materials science forum*, 1997, vol. 246, pp. 105–152.
- [7] J. H. Je, E. Gyarmati, and A. Naoumidis, "Scratch adhesion test of reactively sputtered TiN coatings on a soft substrate," vol. 136, pp. 57–67, 1986.
- [8] S. V Hainsworth, S. J. Bull, and T. F. Page, "Scratch Deformation Response of Thin Cnx Coatings at Ultra-Low Loads," *MRS Online Proc. Libr.*, vol. 522, p. null–null, 1998.
- [9] ASTM, "ASTM C1624 Standard test method for adhesion strength and mechanical failure modes of ceramic coatings by quantitative single point scratch testing," 2015.

- [10] F. Wredenberg and P. L. Larsson, "Scratch testing of metals and polymers: Experiments and numerics," *Wear*, vol. 266, no. 1–2, pp. 76–83, 2009.
- [11] S. C. Bellemare, M. Dao, and S. Suresh, "Effects of mechanical properties and surface friction on elasto-plastic sliding contact," *Mech. Mater.*, vol. 40, no. 4–5, pp. 206–219, 2008.
- [12] X. Hou and N. M. Jennett, "Application of a modified slip-distance theory to the indentation of single-crystal and polycrystalline copper to model the interactions between indentation size and structure size effects," *Acta Mater.*, vol. 60, pp. 4128–4135, 2012.
- [13] I. J. Spary, A. J. Bushby, and N. M. Jennett, "On the indentation size effect in spherical indentation," *Philosophical Magazine*, vol. 86, pp. 5581–5593, 2006.
- [14] X. D. Hou, a J. Bushby, and N. M. Jennett, "Study of the interaction between the indentation size effect and Hall–Petch effect with spherical indenters on annealed polycrystalline copper," *J. Phys. D. Appl. Phys.*, vol. 41, no. 7, p. 074006, Apr. 2008.
- [15] B. D. Beake and T. W. Liskiewicz, "Comparison of nano-fretting and nano-scratch tests on biomedical materials," *Tribol. Int.*, vol. 63, pp. 123–131, 2013.
- [16] ASTM, "ASTM G171 Standard Test Method for Scratch Hardness of Materials Using a Diamond Stylus," *ASTM Stand.*, vol. 03, 2009.
- [17] BS EN ISO 14577-1:2002, "ISO 14577 Metallic materials - instrumented indentation test for hardness and materials parameters," 2002. Published by BSI, 389 Chiswick High Road, London W4 4AL, UK. ISBN 0 580 40792 6
- [18] W. C. Oliver and G. M. Pharr, "An improved technique for determining hardness and elastic modulus using load and displacement sensing indentation experiments," *Journal of Materials Research*, vol. 7, pp. 1564–1583, 1992.
- [19] J. L. Bucaille and E. Felder, "Finite-element analysis of deformation during indentation and scratch tests on elastic-perfectly plastic materials," *Philos. Mag. A*, vol. 82, no. 10, pp. 2003–2012, 2002.

## Appendices

### 1. Resolved force, $F_r$ , calculation.

Figure 10 shows how the resolved force was calculated for each of the tip orientations.

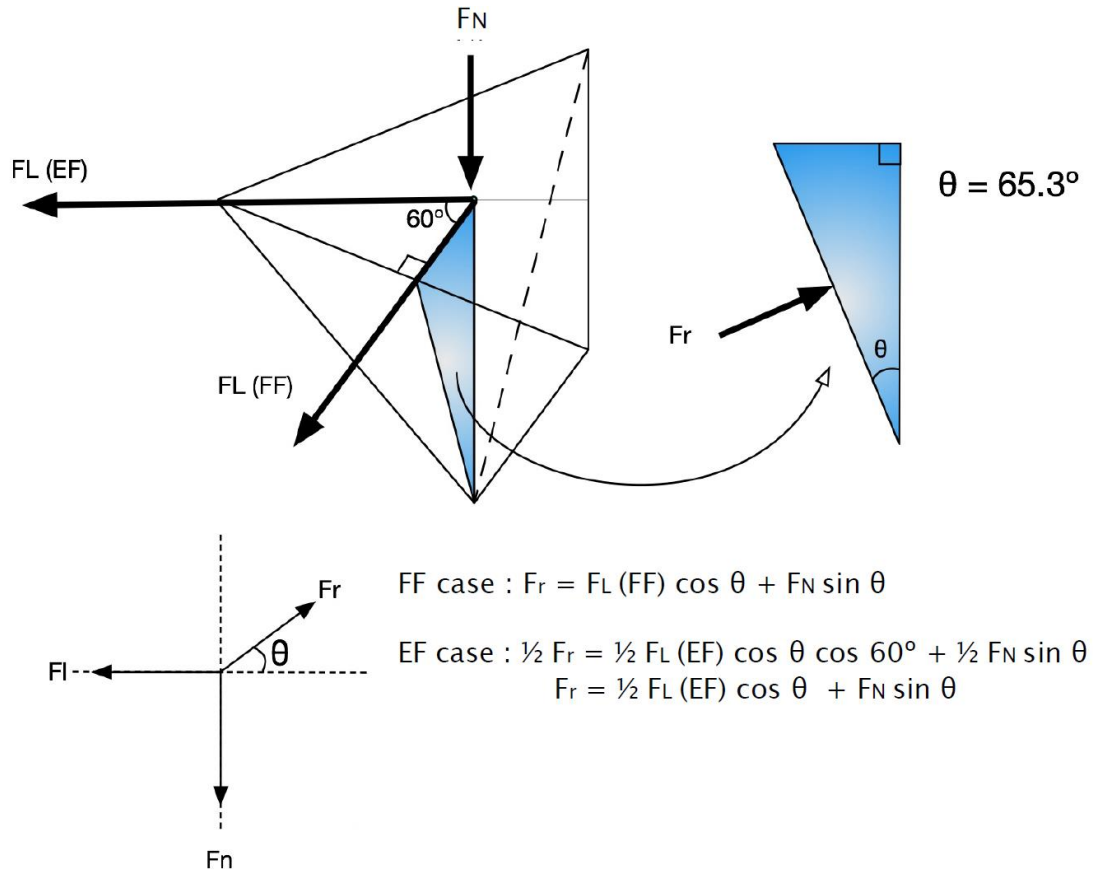


**Figure 10: Resolved force calculation for forces acting on the facets in contact with material for the EF and FF tip orientation. Calculations based on the geometry of the tip,  $F_N$  and  $F_L$  were measured from the instrument.**

## 2. Lateral force, $F_L$ , measurement

The LFM probes measure the deflection of the indenter shaft, relative to its normal x and y position. This is shown in Figure 11;  $K_L$  represents the stiffness of the spring supporting the shaft and  $F$  is the lateral force.

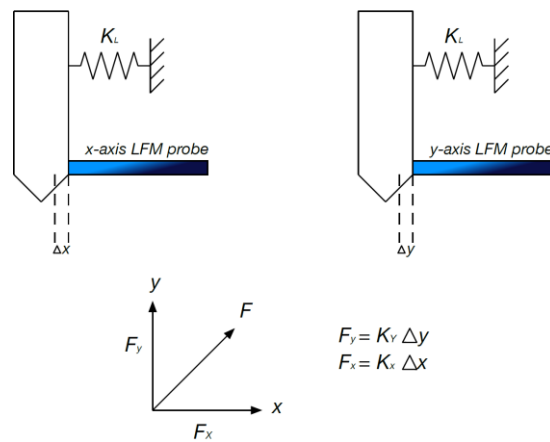


**Figure 11: Lateral force measurement probes showing how the lateral force was determined using measurements of the x and y deflection of the shaft.**